analytical chemistry

Article

pubs.acs.org/ac

Differential Electrochemical Mass Spectrometer Cell Design for Online Quantification of Products Produced during Electrochemical Reduction of CO_2

Ezra L. Clark,[†,‡] Meenesh R. Singh,[†] Youngkook Kwon,[†] and Alexis T. Bell*[,†,‡]

[†]Joint Center for Artificial Photosynthesis, Lawrence Berkeley National Laboratory, Berkeley, California 94720, United States

[‡]Department of Chemical and Biomolecular Engineering, University of California, Berkeley, California 94720-1462, United States

Supporting Information

ABSTRACT: The discovery of electrocatalysts that can efficiently reduce CO_2 to fuels with high selectivity is a subject of contemporary interest. Currently, the available analytical methods for characterizing the products of CO_2 reduction require tens of hours to obtain the dependence of product distribution on applied potential. As a consequence, there is a need to develop novel analytical approaches that can reduce this analysis time down to about an hour. We report here the design, construction, and operation of a novel differential electrochemical mass spectrometer (DEMS) cell geometry that enables the partial current densities of volatile electrochemical reaction products to be quantified in real time. The capabilities of the novel DEMS cell design are demonstrated by carrying out the electrochemical reduction of CO_2 over polycrystalline copper. The reaction products are quantified in real time as a function of the applied potential during linear sweep voltammetry, enabling the product spectrum produced by a given electrocatalyst to be determined as a function of applied potential on a time scale of roughly 1 h.

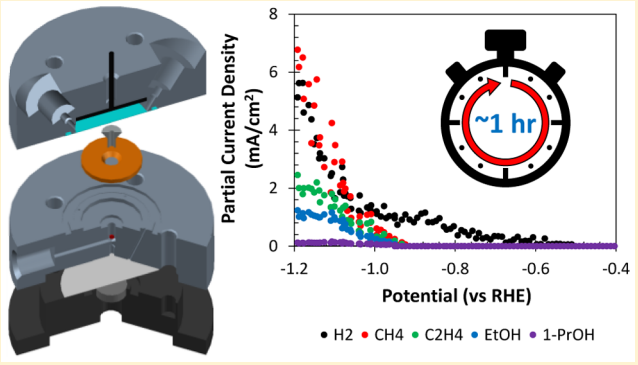

The prospect of utilizing solar energy to promote the electrochemical or photoelectrochemical reduction of CO_2 to transportation fuels has motivated extensive research aimed at identifying highly active and selective electrocatalysts for CO_2 reduction (CO_2R).[1−4] These efforts have revealed that copper is the only metallic electrocatalyst capable of reducing CO_2 to hydrocarbons and alcohols.[5−7] Unfortunately, the reaction requires an overpotential of approximately −1 V or more, resulting in a cathodic CO_2R energy efficiency of less than 25% (see Supporting Information section 1).[8−11] It has also been observed that metallic copper produces up to 16 different products, depending on the surface morphology and the applied potential.[10,11] As a consequence, a great deal of attention is being devoted to the discovery of novel electrocatalysts that can reduce CO_2 to fuels with higher efficiency and a more narrowly defined product spectrum than can be achieved with metallic copper.

A combination of analytical techniques must be employed to fully characterize the products of CO_2R because the reaction produces both gaseous and liquid-phase products.[8,10] Gas chromatography has been used to quantify the gaseous products by periodically sampling the headspace of the electrochemical cell over the course of electrolysis. Liquid-phase products are analyzed after electrolysis by either high-performance liquid chromatography (HPLC) or nuclear magnetic resonance (NMR).[8,10] While gas chromatography is sufficiently sensitive to quantify gaseous products from the effluent of an electrochemical cell, constant-potential electrolysis must be performed for roughly 1 h in order to reach the detection limits of HPLC or NMR because the Faradaic efficiencies of most liquid-phase products are less than 1%.[10] Due to the reliance on chromatography for product analysis, the dependence of the activity and selectivity of CO_2R electrocatalysts has not been studied extensively as a function of time. This is an issue because CO_2R has been reported to be highly sensitive to electrocatalyst deactivation.[12−18] Therefore, there is considerable interest in the development of an analytical technique capable of continuously quantifying generation rates of the major reaction products in both phases in real time. The availability of such a technique would enable the potential dependence of the major reaction products to be determined rapidly by simply sweeping the applied potential and recording the product generation rates in real time. With this objective in mind, Koper and co-workers[19] have developed a micrometer-sized sampling tip that can be placed close to an electrode surface in order to periodically collect liquid-phase reaction for ex situ analysis using HPLC. While this technique

Received: June 2, 2015
Accepted: July 8, 2015
Published: July 8, 2015

DOI: 10.1021/acs.analchem.5b02080
Anal. Chem. 2015, 87, 8013−8020

is well-suited for detecting the presence of liquid-phase reaction products with a more rapid sampling rate, it cannot be used to quantify the Faradaic efficiencies of these products due to the low collection efficiency of the product.

Differential electrochemical mass spectrometry (DEMS) is an analytical technique that utilizes pervaporation to continuously separate and collect electrochemical reaction products.[20] Because the analysis time of mass spectrometry is on the order of a second, the generation rates of gaseous or volatile reaction products can be quantified in real time by recording the relevant mass ion currents and relating them to the partial current densities of the corresponding reaction products.[20] Koper and co-workers[21] developed an online electrochemical mass spectrometer (OLEMS) capable of detecting the hydrocarbon products of CO_2R in real time using a sampling tip placed in close proximity with the electrode surface. In related work, Mayrhofer and co-workers[22] have recently reported the design of a novel DEMS cell capable of detecting the hydrocarbon products of CO_2R that can also be used to raster an electrode surface with varying composition in order to rapidly screen bimetallic CO_2R electrocatalysts. While both approaches can be used to detect the presence of gaseous electrochemical reaction products in real time, neither approach is capable of quantification due to low and ill-defined product collection efficiencies. The collection efficiency of OLEMS is extremely low and highly sensitive to the distance between the sampling tip and the electrode surface, whereas the thin-layer flow cell geometry employed by Mayrhofer and co-workers suffers from low product collection efficiency under electrolyte convection.[23]

The capabilities of DEMS strongly depend on the design of the electrochemical cell, which must be capable of achieving both rapid response time and high product collection efficiency.[23,24] A number of additional design criteria must also be met to enable product quantification. The working and counter electrodes should be parallel to ensure uniform potential distribution across the surface of the electrodes, and they should be separated by an ion-conducting membrane to prevent unwanted parasitic reactions, such as oxidation of CO_2R products or reduction of O_2. Electrolyte convection must be employed for two reasons: (1) to ensure that the electrolyte does not become depleted of CO_2 and (2) to provide good mass transfer to and away from the cathode (see Supporting Information section 2). It is also necessary to isolate the working electrode from the pervaporation membrane because significant CO_2 depletion will occur due to pervaporation through the collection membrane if it is in the vicinity of the working electrode. As a result, the electrolyte volume between the working electrode and the pervaporation membrane must be minimized so that an acceptable delay time between product generation and detection can be achieved without diluting the liquid-phase reaction products beyond the limits of detection. Finally, the surface area of the working electrode should be large so that the concentration of liquid-phase products can be maximized.

DEMS cell designs described in the literature preclude product quantification, primarily as a consequence of either poorly defined electrochemistry or low product collection efficiencies.[21,25] The dual thin-layer flow cell is capable of achieving liquid-phase product collection efficiencies as high as 40% by locating the working electrode and pervaporation membrane in separate chambers.[24] By minimizing the overall cell volume, delay times of ~2 s were achieved. However, the design suffers from a nonparallel electrode configuration and high cell resistance (~10 kΩ) due to the capillary tube connecting the working and counter electrode chambers.[23,24] The high cell resistance makes it impossible to drive CO_2R to hydrocarbons and alcohols using polycrystalline copper without first reaching the compliance voltage of modern potentiostats. To the best of our knowledge, there have been no reports in the literature of using DEMS to detect the liquid-phase products of CO_2R or to quantify any reaction products in real time.[13,16,22,26−32] The objective of the work reported here was to design and construct a DEMS cell that meets all of the criteria noted above and to demonstrate its performance by conducting CO_2R over a polycrystalline copper cathode.

EXPERIMENTAL SECTION

DEMS Cell Design and Construction. A schematic of the DEMS cell is depicted in Figure 1. The catholyte enters the working electrode chamber through the center of a washer-shaped electrode with an exposed surface area of 1 cm^2. The catholyte rapidly reaches the ion-conducting membrane, which is separated from the working electrode surface by a thin layer of electrolyte approximately 130 μm thick. The catholyte then flows radially outward toward the four transfer capillaries, which connect the working electrode and collection chambers. Figure 2 shows the details of the working electrode chamber, which has a total catholyte volume of roughly 25 μL. The reference electrode intercepts the catholyte stream at the base of the working electrode mounting screw, which also serves as the electrolyte inlet to the working electrode chamber. By locating the reference electrode outside the working electrode chamber, the impact of gaseous product bubble formation on the potential referencing of the working electrode is minimized. A third chamber, located above the working electrode chamber, houses the counter electrode such that a parallel electrode configuration is achieved. The counter electrode is a mesh disc

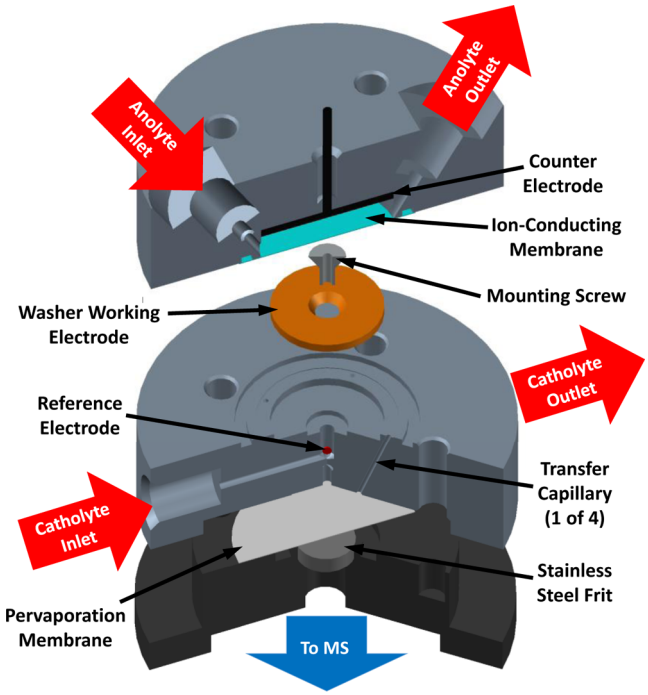

Figure 1. Schematic of DEMS cell.

DOI: 10.1021/acs.analchem.5b02080
Anal. Chem. 2015, 87, 8013−8020

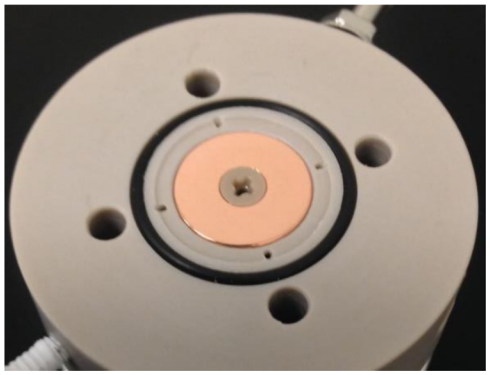

Figure 2. Photograph of working electrode chamber.

with an exposed surface area of roughly 2 cm^2. The electrolyte is pumped from a shared reservoir through both electrode chambers at the same flow rate by a set of identical syringe pumps. The surface area of the ion-conducting membrane separating the two electrode chambers is roughly 1.75 cm^2. As a result of these design decisions, the DEMS cell has a low cell resistance (~50 Ω), robust electrode connectivity, and minimal overpotential at the counter electrode, which enables the potentials required to produce hydrocarbons and alcohols over polycrystalline copper to be experimentally accessible. Additional photographs of the DEMS cell and a table of specifications can be found in the Supporting Information (sections 3 and 4).

The working and counter electrode chambers were fabricated of polyether ether ketone (Professional Plastics) and polycarbonate (McMaster–Carr), respectively, and were fitted with Viton O-rings (McMaster–Carr). The cell was treated with UV-generated ozone to reduce the wetting angle of the electrolyte on the exposed surfaces of the cell, which reduces the holdup of gaseous product bubbles in the working electrode chamber (see Supporting Information section 5). The working electrode was machined from a copper sheet (99.999%, Sigma–Aldrich). Prior to each experiment, the copper surface was polished mechanically with a diamond polishing compound to a mirrorlike finish (0.1 μm, Ted Pella Inc.). The counter electrode was a platinum gauze disc (100 mesh, 99.9% Sigma–Aldrich) that was flame-annealed prior to each experiment. A Ag/AgCl electrode was used as the reference (1 mm o.d., Innovative Instruments Inc.). A proton-conducting membrane (Nafion 110, Ion Power Inc.) was used as the ion-conducting membrane. Attempts were made to use an anion-conducting membrane (Selemion AMV, AGC Inc.) but they were not successful due to gaseous product bubble holdup on the membrane surface that severely disrupted the electrochemical measurements. A poly(tetrafluoroethylene) (PTFE) sheet (20 nm pore size, Hangzhou Cobetter Filtration Equipment Co.) was used as the pervaporation membrane. A 0.05 M K_2CO_3 (99.995%, Sigma–Aldrich) solution prepared with 18.2 MΩ deionized water from a Millipore system was used as the electrolyte. After saturation with CO_2 (99.999%, Praxair) at 25 °C, the steady-state pH of the electrolyte was 6.8, making it chemically equivalent to a 0.1 M $KHCO_3$ solution saturated with CO_2 at the same temperature (see Supporting Information section 6).

Electrochemistry. Electrochemistry was performed on a Biologic VSP-300 potentiostat. All electrochemical data were recorded versus the reference electrode and converted to the reversible hydrogen electrode (RHE) scale by use of the relationship $E_{RHE} = E_{Ag/AgCl} + 0.197 + 0.059(pH_{bulk})$. A 5 Hz filter was used to eliminate noise from the working electrode potential measurement caused by the flow of electrolyte. Prior to each experiment, the potential applied to the working electrode was swept from open circuit to −1 V versus RHE at 50 mV/s in order to reduce the native CuO_x layer. Potentiostatic electrochemical impedance spectroscopy (PEIS) was then used to determine the total uncompensated resistance (R_u) by applying frequencies from 10 Hz to 30 kHz at the open circuit potential (see Supporting Information section 7). The potentiostat compensated for 85% of R_u in situ, and the last 15% was postcorrected to arrive at accurate potentials. The potential applied to the working electrode was then swept from open circuit to −1.2 V versus RHE at 0.2 mV/

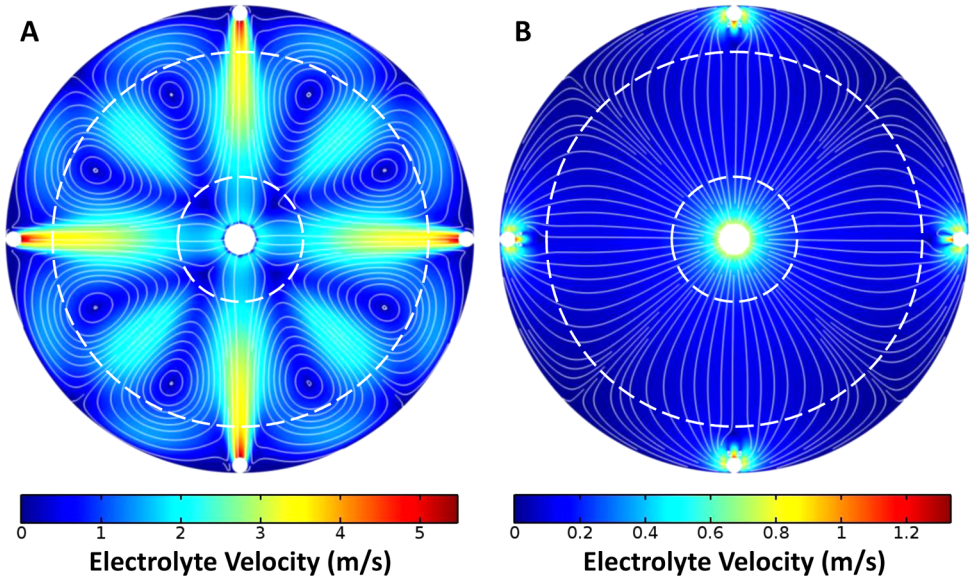

Figure 3. Catholyte flow field in the working electrode chamber at a flow rate of 1 mL/min for convection driven by (A) positive pressure applied at the inlet and (B) negative pressure applied at the outlet. The working electrode surface is denoted by the region between the dashed white lines.

DOI: 10.1021/acs.analchem.5b02080
Anal. Chem. 2015, 87, 8013–8020

s. This scan rate was determined experimentally to be optimal for reducing the impact of bubble noise on the recorded mass ion current trends (see Supporting Information section 8). The linear potential sweep was repeated twice, and only the second scan was used for further analysis.

Product Detection by Mass Spectrometry. Mass spectra were acquired on a Hiden HPR40 dissolved-species mass spectrometer. An electron energy of 70 eV was used for ionization of all species, with an emission current of 500 μA. Hydrogen ions (m/z = 2) were accelerated with a voltage of 1.3 V to prevent detector saturation, while methane (m/z = 15), ethene (m/z = 26), and ethanol/1-propanol (m/z = 31) ions were accelerated with a voltage of 3 V to maximize the detector response. All mass-selected product cations were detected by a secondary electron multiplier with a detector voltage of 1200 V. These mass spectrometer settings were determined to be optimal for maximizing the signal-to-noise ratio of the liquid-phase products while not overloading the detector with H_2 (see Supporting Information section 9). With these settings, a data point was recorded every 1.4 s. The data were averaged over 10 mV increments during linear sweep voltammetry and over 1 min intervals during chronoamperometry in order to minimize the influence of bubble noise on the recorded trends.

RESULTS AND DISCUSSION

Electrolyte Flow Rate and CO_2R Product Detectability. The flow pattern and average residence time of the catholyte in the working electrode were found to influence cell performance and liquid-phase product detectability. First, the convection of the catholyte driven by either positive pressure applied at the cell inlet or negative pressure applied at the cell outlet was examined. In the first case, the formation of recirculation eddies led to an increase in the holdup of gaseous product bubbles in the working electrode chamber, which caused erratic current flow due to partial blockage of catholyte access to the electrode surface. These difficulties were eliminated when electrolyte convection was driven by negative pressure applied at the cell outlet. To support these observations, the electrolyte velocity field across the working electrode chamber was simulated for convection driven by both positive and negative pressure (see Supporting Information section 10). As shown in Figure 3, the simulations confirm the existence of recirculation eddies in the case of electrolyte convection driven by positive pressure. However, these eddies do not form when electrolyte convection is driven by negative pressure. For this reason, negative pressure was employed to supply the electrolyte.

It is important that the average residence time of the electrolyte in the working electrode chamber be neither too short nor too long. Too short a residence time will lead to insufficient product accumulation in the electrolyte stream, thereby reducing the detectability of products of interest. Conversely, too long a residence time will cause an accumulation of gaseous product bubbles in the working electrode chamber and a depletion of dissolved CO_2, which may result in mass-transfer limitations. Ideally, the average residence time should be equivalent to the time interval over which mass spectrometry data will be acquired. To this end, the residence time distribution of the catholyte passing through the working electrode chamber and the transfer capillaries was calculated as a function of flow rate by solving the Navier–Stokes and mass-balance equations in COMSOL Multiphysics v4.3b (see Supporting Information section 10). As shown in Figure 4, the calculations indicate that a flow rate of at least 0.5

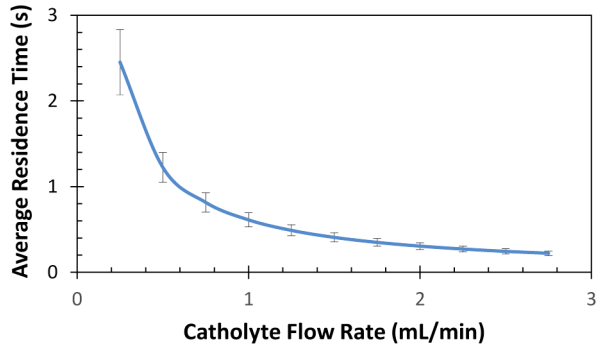

Figure 4. Average residence time and distribution (error bars) of catholyte in the working electrode chamber as a function of electrolyte flow rate.

mL/min is required to achieve an average residence time on the order of the analysis time of the mass spectrometer (~1.5 s). However, there is a wide standard deviation in the residence time at this flow rate, as indicated by the error bars, which reduces the accuracy of liquid-phase product quantification. To reduce this uncertainty, a minimum flow rate of 1 mL/min was selected. The maximum volumetric generation rate of gaseous products produced by use of polycrystalline copper was calculated to be less than 100 μL/min at potentials positive of −1.2 V versus RHE (see Supporting Information section 11). Thus, there should be no issues with gaseous product accumulation inside the cell chambers at the minimum flow rate selected.

All gaseous CO_2R products are detectable by DEMS except CO. CO is undetectable because its ionization produces the same mass fragments as CO_2, which is present in the electrolyte at a concentration at least 3 orders of magnitude higher than CO at the minimum electrolyte flow rate (see Supporting Information section 12). To estimate the detection limit of liquid-phase products, increasingly concentrated ethanol and 1-propanol solutions were fed into the cell at 1 mL/min. The limit of detection was defined as the concentration of these species that resulted in a mass ion current signal equal to the magnitude of the standard deviation of the baseline signal. By this means, the liquid-phase product detection limit was determined to be ~5 μM (see Supporting Information section 13). According to the current literature, the only liquid-phase products with generation rates high enough to reach this concentration at the minimum electrolyte flow rate are formic acid, ethanol, and 1-propanol (see Supporting Information section 14). However, formic acid is undetectable, since this species is fully dissociated and hence cannot pervaporate into the mass spectrometer at the pH of the electrolyte. The inability to detect formic acid was verified experimentally with a formic acid solution 2 orders of magnitude more concentrated than expected to be observed during CO_2R at the minimum electrolyte flow rate (see Supporting Information section 15).

Only signal from the primary ionization fragment of ethanol and 1-propanol (m/z = 31) was observable during CO_2R over polycrystalline copper at the minimum electrolyte flow rate. This is an issue because cations with this m/z ratio are also produced by methanol, glycolaldehyde, ethylene glycol, allyl alcohol, and propionaldehyde. However, based on previous literature reports, only ethanol and 1-propanol will contribute significantly to the m/z = 31 signal, since the Faradaic efficiencies of the other products do not exceed 2% (see Supporting Information section 16).[8,10] In principle, it should

DOI: 10.1021/acs.analchem.5b02080
Anal. Chem. 2015, 87, 8013−8020

be possible to deconvolute the contributions to the m/z = 31 signal made by ethanol and 1-propanol by use of the mass ion currents associated with their secondary ionization fragments. However, the secondary ionization fragment produced by ethanol (m/z = 46) overlaps with that from $^{12}C^{18}O_2$, resulting in an erratic baseline that prevents clear trends from being observed (see Supporting Information section 17). Furthermore, the concentration of 1-propanol expected to be formed by the reaction is insufficient to reach the detection limit of its secondary ionization fragment (m/z = 59) (see Supporting Information section 17). In order to determine the contribution of ethanol and 1-propanol to the m/z = 31 signal, their generation rates over polycrystalline copper were measured at a series of increasingly negative potentials in a conventional H-type cell. After electrolysis, the composition of the catholyte was measured by HPLC, and the relative concentration of ethanol to 1-propanol was plotted as a function of applied potential (see Supporting Information section 18). The linear relationship was then used to deconvolute the m/z = 31 signal as a function of potential so that the generation rates of both alcohols could be determined in real time, assuming that they are both uniformly distributed in the catholyte entering the collection chamber.

Product Quantifiability. Linear sweep voltammetry was conducted in a He-sparged electrolyte (pH = 11.3) so that the ion current for m/z = 2 could be related directly to the hydrogen generation rate. As shown in Figure 5A,B, the total current density and ion current for m/z = 2 track each other as a function of potential under these conditions. This clearly demonstrates that a recorded mass ion current can be related directly to the generation rate of the corresponding product.[20] As shown in Figure 5B,C, a discontinuity in the m/z = 2 signal response and a sudden increase in the standard deviation are observed at −0.6 V versus RHE. The current density corresponding to this potential was calculated to result in saturation of the electrolyte with hydrogen (see Supporting Information section 19). Thus, positive of −0.6 V versus RHE, the hydrogen is entirely dissolved and hence no change is observed in the standard deviation of the ion current for m/z = 2 versus the baseline standard deviation. However, at potentials negative of −0.6 V versus RHE, the hydrogen saturates the electrolyte and forms bubbles, causing a sudden increase in standard deviation of the ion current for m/z = 2. Chronopotentiometry was conducted for 10 min at increasingly negative current densities in order to establish the m/z = 2 calibration curve for the case of He-sparged electrolyte. As shown in Figure 6, distinct calibration regimes were observed for dissolved and gaseous hydrogen. The signal response is greater for gaseous hydrogen because the collection efficiency of a gaseous product is higher than that of a dissolved product. Thus, it is imperative to use the standard deviation of the recorded mass ion currents to identify which phase the detected products are in, so that accurate quantification can be performed.

Rapid Electrocatalyst Screening via Linear Sweep Voltammetry. Linear sweep voltammetry was conducted in a CO_2-sparged electrolyte to demonstrate the ability of the DEMS cell to quantify the generation rates of multiple electrochemical reaction products in real time. The recorded voltammogram, shown in Figure 7, closely matches that reported by Jaramillo and co-workers[10] at potentials positive of −1.2 V versus RHE, indicating that the cell geometry does not significantly impact the electrochemistry up to this

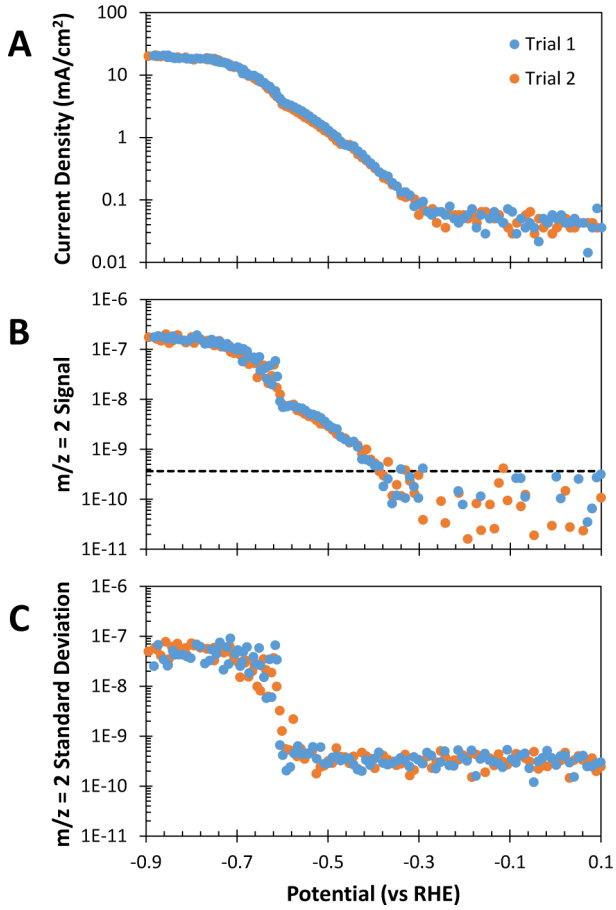

Figure 5. DEMS results obtained in a He-sparged 0.05 M K_2CO_3 electrolyte (pH = 11.3) with an electrolyte flow rate of 1 mL/min and a scan rate of 1 mV/s. (A) Current density; (B) m/z = 2 signal; (C) m/z = 2 standard deviation.

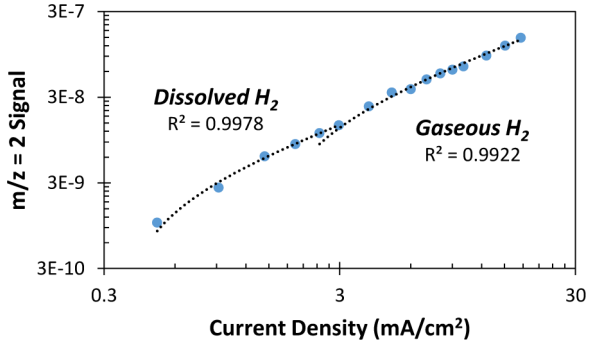

Figure 6. m/z = 2 calibration curve for a He-sparged electrolyte.

potential. At potentials more negative than −1.2 V versus RHE, a suppression in the current density is observed that is a result of inadequate gaseous product bubble clearing from the working electrode surface. At the potentials of gaseous product detection onset, standard deviations of the corresponding ion currents increased versus standard deviation of the baselines (see Supporting Information section 20). This pattern, which was absent for m/z = 31, indicates that the detected gaseous products have phase-segregated from the aqueous electrolyte at these potentials. Thus, the ion currents corresponding to the gaseous products were calibrated by introducing a standard gas containing hydrogen, methane, and ethene into the catholyte

DOI: 10.1021/acs.analchem.5b02080
Anal. Chem. 2015, 87, 8013−8020

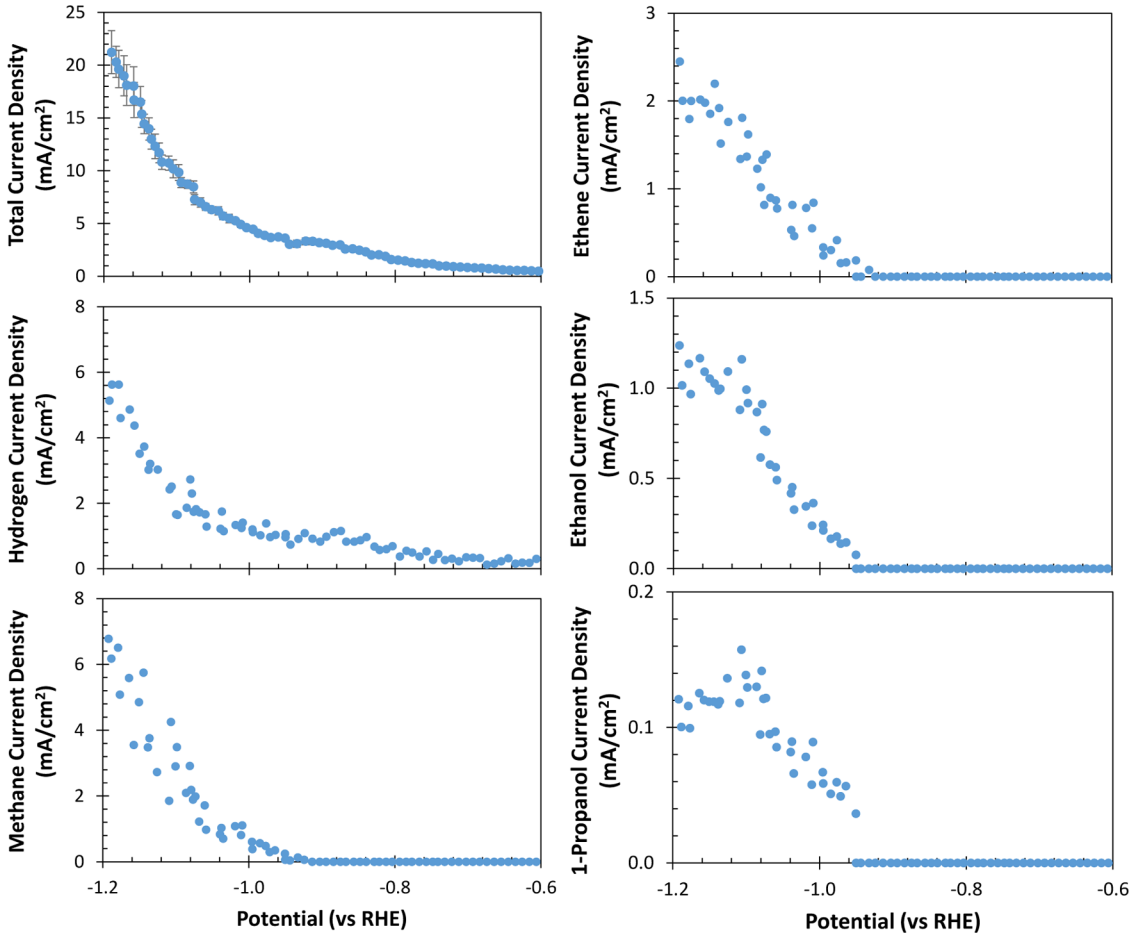

Figure 7. DEMS results obtained for CO_2-sparged 0.05 M K_2CO_3 electrolyte (pH = 6.8) with an electrolyte flow rate of 1 mL/min and a scan rate of 0.2 mV/s.

stream at a series of defined flow rates (see Supporting Information section 21). This calibration methodology simulates the formation of gaseous product bubbles at the working electrode surface because the standard gas bubbles are completely removed from the catholyte stream in the collection chamber, enabling mass ion current signals corresponding to the gaseous products to be directly related to the flux of individual chemical species entering the collection chamber. The signal response for m/z = 2 obtained by this approach matched the gaseous hydrogen calibration curve obtained electrochemically in a He-sparged electrolyte, indicating that this calibration methodology is accurate because it produces the same signal response that is observed electrochemically.

The partial current potential dependence of hydrogen, methane, ethene, ethanol, and 1-propanol recorded during the linear potential sweep are shown in Figure 7. While the recorded data exhibit trends similar to those previously reported[8,10,33] (see Supporting Information section 22), two major discrepancies exist: (1) the total current density is higher at potentials positive of the onset of hydrocarbon and alcohol detection, and (2) the partial current densities of the C_{2+} products do not decline at potentials negative of −1.1 V versus RHE. Both of these discrepancies can be explained by the use of electrolyte convection, which increases the CO_2 concentration and minimizes the CO_2R product concentrations in the vicinity of the cathode. The adsorption of CO onto the copper surface is known to result in potential-dependent deactivation.[8,34,35] By minimizing the concentration of CO in the vicinity of the cathode, a higher CO desorption rate is achieved, which reduces the extent of CO poisoning at potentials positive of the onset of hydrocarbons and alcohols. Recent modeling efforts suggest that a significant increase in the pH and a depletion of dissolved CO_2 occur within the hydrodynamic boundary layer at the surface of a polycrystalline copper cathode at potentials negative of −1 V versus RHE despite vigorous electrolyte mixing.[36] These losses cause the measured electrocatalytic activity and selectivity to differ from those that would be observed in the absence of electrolyte polarization and mass-transfer limitations. The DEMS cell employed in this study minimizes these polarization and mass-transfer effects by virtue of the continuous flow of electrolyte, which reduces the hydrodynamic boundary layer thickness and continuously supplies the electrode surface with CO_2. This is why partial current densities of the C_{2+} products do not decline at potentials more negative than −1.1 V vs RHE. This hypothesis is further supported by suppression of the hydrogen evolution reaction (HER) observed at these potentials by use of the DEMS cell. Thus, the DEMS cell described here is superior to conventional mixed-electrolyte cells for measuring intrinsic electrocatalytic activities and selectivities at high current densities.

Measuring Transient Selectivity via Chronoamperometry. There have been no reports in the literature demonstrating changes in the selectivity of CO_2R to C_{2+}

DOI: 10.1021/acs.analchem.5b02080
Anal. Chem. 2015, 87, 8013−8020

liquid-phase products as a function of time. This is an issue because the selectivity to C_{2+} products has been reported to be extremely sensitive to the presence of impurities in the electrolyte, such as iron and zinc, that quickly contaminate the copper surface at the potentials required to drive CO_2R to hydrocarbons and alcohols.[18,37] Currently, liquid product selectivity is quantified at the end of the reaction, and it is assumed that no deactivation occurs over the course of ∼1 h electrolysis. However, the validity of this assumption has not been substantiated experimentally due to the lack of an analytical technique capable of quantifying the transient generation rates of C_{2+} liquid-phase products in real time. To fill this void, chronoamperometry was conducted at −1.14 V versus RHE for 1 h. As shown in Figure 8, no substantial

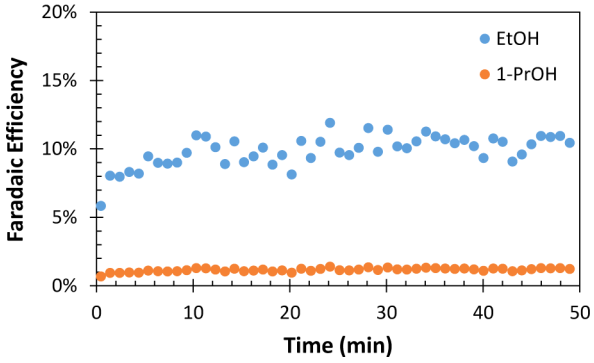

Figure 8. Transient ethanol and 1-propanol Faradaic efficiencies recorded during chronoamperometry at −1.14 V versus RHE in a CO_2-sparged 0.05 M K_2CO_3 electrolyte (pH = 6.8) with an electrolyte flow rate of 1 mL/min.

change in the ethanol or 1-propanol Faradaic efficiency was observed over the course of electrolysis. Furthermore, the Faradaic efficiencies of the other detectable reaction products were constant over the electrolysis period (see Supporting Information section 23). These results suggest that deactivation of the copper electrode is not an issue as long as high-purity reagents are used to prepare the electrolyte.

CONCLUSIONS

In conclusion, a DEMS cell has been designed that satisfies all the criteria required to achieve meaningful product quantification in real time. These criteria include parallel electrode configuration, high product collection efficiencies, and rapid response time. The efficacy of the cell was demonstrated by performing CO_2R over polycrystalline copper and quantifying the generation rates of both gaseous and liquid-phase products during a linear potential sweep and at a fixed potential as a function of time. To the best of our knowledge, this effort represents the first example of DEMS being used to quantify all major products of CO_2R, with the exception of CO and formic acid. The potential dependence of partial current densities of the detectable reaction products matched the trends reported by other workers[8,10,33] but were obtained on the time scale of an hour rather than the tens of hours required for conventional analytical approaches. It was also demonstrated that the copper electrocatalyst experiences no deactivation over the course of 1 h of electrolysis at a fixed potential when pure reagents are used to prepare the electrolyte. This is the first time that the transient selectivity of CO_2R to C_{2+} liquid-phase products has been reported in the literature. The DEMS cell developed and described in this study is currently being used to screen the activity and selectivity of novel electrocatalysts as a function of potential and to investigate changes in their activity and selectivity over time.

ASSOCIATED CONTENT

Supporting Information

Additional text, 28 equations, 33 figures, and five tables, organized into 23 sections as described in the main text. This material is available free of charge via the Internet at http://pubs.acs.org/.The Supporting Information is available free of charge on the ACS Publications website at DOI: 10.1021/acs.analchem.5b02080.

AUTHOR INFORMATION

Corresponding Author

*E-mail alexbell@berkeley.edu.

Notes

The authors declare no competing financial interest.

ACKNOWLEDGMENTS

This material is based upon work performed by the Joint Center for Artificial Photosynthesis, a DOE Energy Innovation Hub, supported through the Office of Science of the U.S. Department of Energy under Award DE-SC0004993. E.L.C. is supported by the National Science Foundation (NSF). We also acknowledge Professor Tom Jaramillo, Dr. Mary Louie, Eric Granlund, Etosha Cave, and Gerry Duffy for contributions made through helpful discussions.

REFERENCES

(1) Jitaru, M.; Lowy, D. A.; Toma, M.; Toma, B. C.; Oniciu, L. *J. Appl. Electrochem.* **1997**, *27*, 875−889.
(2) Gattrell, M.; Gupta, N.; Co, A. *J. Electroanal. Chem.* **2006**, *594*, 1−19.
(3) Hori, Y. In *Modern Aspects of Electrochemistry*, Vol. *42*; Vayenas, C. G., White, R. E., Gamboa-Aldeco, M. E., Eds.; Springer: New York, 2008; pp 89−189.
(4) Whipple, D. T.; Kenis, P. J. A. *J. Phys. Chem. Lett.* **2010**, *1*, 3451−3458.
(5) Hori, Y.; Kikuchi, K.; Suzuki, S. *Chem. Lett.* **1985**, 1695−1698.
(6) Noda, H.; Ikeda, S.; Oda, Y.; Imai, K.; Maeda, M.; Ito, K. *Bull. Chem. Soc. Jpn.* **1990**, *63*, 2459−2462.
(7) Hori, Y.; Wakebe, H.; Tsukamoto, T.; Koga, O. *Electrochim. Acta* **1994**, *39*, 1833−1839.
(8) Hori, Y.; Murata, A.; Takahashi, R. *J. Chem. Soc., Faraday Trans. 1* **1989**, *85*, 2309−2326.
(9) Peterson, A. A.; Abild-Pedersen, F.; Studt, F.; Rossmeisl, J.; Nørskov, J. K. *Energy Environ. Sci.* **2010**, *3*, 1311−1315.
(10) Kuhl, K. P.; Cave, E. R.; Abram, D. N.; Jaramillo, T. F. *Energy Environ. Sci.* **2012**, *5*, 7050−7059.
(11) Tang, W.; Peterson, A. a; Varela, A. S.; Jovanov, Z. P.; Bech, L.; Durand, W. J.; Dahl, S.; Nørskov, J. K.; Chorkendorff, I. *Phys. Chem. Chem. Phys.* **2012**, *14*, 76−81.
(12) DeWulf, D. W.; Jin, T.; Bard, A. J. *J. Electrochem. Soc.* **1989**, *136*, 1686−1691.
(13) Wasmus, S.; Cattaneo, E.; Vielstich, W. *Electrochim. Acta* **1990**, *35*, 771−775.
(14) Kyriacou, G.; Anagnostopoulos, A. *J. Electroanal. Chem.* **1992**, *322*, 233−246.
(15) Shiratsuchi, R.; Aikoh, Y.; Nogami, G. *J. Electrochem. Soc.* **1993**, *140*, 3479−3482.
(16) Friebe, P.; Bogdanoff, P.; Alonso-Vante, N.; Tributsch, H. *J. Catal.* **1997**, *168*, 374−385.
(17) Lee, J.; Tak, Y. *Electrochim. Acta* **2001**, *46*, 3015−3022.

DOI: 10.1021/acs.analchem.5b02080
Anal. Chem. 2015, 87, 8013−8020

(18) Hori, Y.; Konishi, H.; Futamura, T.; Murata, A.; Koga, O.; Sakurai, H.; Oguma, K. *Electrochim. Acta* **2005**, *50*, 5354−5369.
(19) Kwon, Y.; Koper, M. T. M. *Anal. Chem.* **2010**, *82*, 5420−5424.
(20) Wolter, O.; Heitbaum, J. *Berichte der Bunsengesellschaft für Phys. Chemie* **1984**, *88*, 2−6.
(21) Wonders, A. H.; Housmans, T. H. M.; Rosca, V.; Koper, M. T. M. *J. Appl. Electrochem.* **2006**, *36*, 1215−1221.
(22) Grote, J.-P.; Zeradjanin, A. R.; Cherevko, S.; Mayrhofer, K. J. J. *Rev. Sci. Instrum.* **2014**, *85*, 104101.
(23) Ashton, S. J. *Design, Construction, and Research Application of a Differential Electrochemical Mass Spectrometer (DEMS)*; Springer: Heidelberg, Germany, 2012; pp 1−111.
(24) Baltruschat, H. *J. Am. Soc. Mass Spectrom.* **2004**, *15*, 1693−1706.
(25) Jusys, Z.; Massong, H.; Baltruschat, H. *J. Electrochem. Soc.* **1999**, *146*, 1093−1098.
(26) Schouten, K. J. P.; Kwon, Y.; van der Ham, C. J. M.; Qin, Z.; Koper, M. T. M. *Chem. Sci.* **2011**, *2*, 1902−1909.
(27) Schouten, K. J. P.; Qin, Z.; Gallent, E. P.; Koper, M. T. M. *J. Am. Chem. Soc.* **2012**, *134*, 9864−9867.
(28) Schouten, K. J. P.; Gallent, E. P.; Koper, M. T. M. *ACS Catal.* **2013**, *3*, 1292−1295.
(29) Schouten, K. J. P.; Gallent, E. P.; Koper, M. T. M. *J. Electroanal. Chem.* **2014**, *716*, 53−57.
(30) Kortlever, R.; Tan, K. H.; Kwon, Y.; Koper, M. T. M. *J. Solid State Electrochem.* **2013**, *17*, 1843−1849.
(31) Reske, R.; Duca, M.; Oezaslan, M.; Schouten, K. J. P.; Koper, M. T. M.; Strasser, P. *J. Phys. Chem. Lett.* **2013**, *4*, 2410−2413.
(32) Kas, R.; Kortlever, R.; Milbrat, A.; Koper, M. T. M.; Mul, G.; Baltrusaitis, J. *Phys. Chem. Chem. Phys.* **2014**, *16*, 12194−12201.
(33) Noda, H.; Ikeda, S.; Oda, Y.; Ito, K. *Chem. Lett.* **1989**, *2*, 289−292.
(34) Hori, Y.; Murata, A.; Yoshinami, Y. *J. Chem. Soc., Faraday Trans.* **1991**, *87*, 125−128.
(35) Hori, Y.; Takahashi, R.; Yoshinami, Y.; Murata, A. *J. Phys. Chem. B* **1997**, *101*, 7075−7081.
(36) Singh, M. R.; Clark, E. L.; Bell, A. T. *Phys. Chem. Chem. Phys.* **2015**, *17*, 18924−18936.
(37) Hori, Y.; Kikuchi, K.; Murata, A.; Suzuki, S. *Chem. Lett.* **1986**, *6*, 897−898.

DOI: 10.1021/acs.analchem.5b02080
Anal. Chem. 2015, 87, 8013−8020